Phase Asymmetry of Andreev Spectra from Cooper-Pair Momentum

Abhishek Banerjee,[1] Max Geier,[1] Md Ahnaf Rahman,[1] Candice Thomas,[2] Tian Wang,[2] Michael J. Manfra,[2,3] Karsten Flensberg,[1] and Charles M. Marcus[1]

[1]*Center for Quantum Devices, Niels Bohr Institute, University of Copenhagen, Universitetsparken 5, 2100 Copenhagen, Denmark*

[2]*Department of Physics and Astronomy, and Birck Nanotechnology Center, Purdue University, West Lafayette, Indiana 47907, USA*

[3]*School of Materials Engineering, and School of Electrical and Computer Engineering, Purdue University, West Lafayette, Indiana 47907, USA*

(Received 4 January 2023; revised 10 August 2023; accepted 16 October 2023; published 9 November 2023)

In analogy to conventional semiconductor diodes, the Josephson diode exhibits superconducting properties that are asymmetric in applied bias. The effect has been investigated in a number of systems recently, and requires a combination of broken time-reversal and inversion symmetries. We demonstrate a dual of the usual Josephson diode effect, a nonreciprocal response of Andreev bound states to a superconducting phase difference across the normal region of a superconductor-normal-superconductor Josephson junction, fabricated using an epitaxial InAs/Al heterostructure. Phase asymmetry of the subgap Andreev spectrum is absent in the absence of in-plane magnetic field and reaches a maximum at 0.15 T applied in the plane of the junction transverse to the current direction. We interpret the phase diode effect in this system as resulting from finite-momentum Cooper pairing due to orbital coupling to the in-plane magnetic field. At higher magnetic fields, we observe a sign reversal of the diode effect that appears together with a reopening of the spectral gap. Within our model, the sign reversal of the diode effect at higher fields is correlated with a topological phase transition that requires Zeeman and spin-orbit interactions in addition to orbital coupling.

DOI: 10.1103/PhysRevLett.131.196301

Nonreciprocal effects in superconducting systems have attracted significant recent interest. A primary motivation is to engineer a superconducting diode, a circuit element that supports dissipationless flow of current in one direction but is resistive in the opposite [1]. Nonreciprocity of supercurrent flow has been observed in thin film superconductors [2–11] and Josephson junction devices [12–17]. In general, nonreciprocal superconductivity requires the breaking of time-reversal and inversion symmetries [18–30], also prerequisites for various topological superconducting states. Nonreciprocal effects may therefore also serve as a marker for unconventional superconducting order [9,10,19,21,31].

Several proposals have been put forward to explain nonreciprocal superconducting transport. In uniform noncentrosymmetric materials, breaking of time-reversal symmetry with a magnetic field generates a nonreciprocal supercurrent [6,23,25–27,29]. In Josephson junctions, various mechanisms may lead to a Josephson diode effect, including spin-orbit coupling with an external magnetic field [18–21], ferromagnetism of the barrier [24,32], and finite-momentum Cooper pairing [13,28,31].

The behavior of Andreev bound states (ABSs) carrying nonreciprocal supercurrents across Josephson junctions has been predicted in the form of an asymmetric energy-phase relationship where $E(\phi_i - \phi) \neq E(\phi_i + \phi)$ for any value of ϕ_i [20,28]. This is different from the ϕ_0 Josephson effect where the ABS spectrum is phase-shifted by ϕ_0 but still remains symmetric about $\phi = \phi_0$ [33–35]. Signatures of weakly phase-asymmetric ABSs have been observed in semiconductor Josephson junctions where this behavior was attributed to spin-orbit coupling [36,37]. Orbital-effect-dominated phase asymmetries were not observed in these experiments, presumably due to the low transverse critical fields (∼10 mT).

Here, we use tunneling spectroscopy to experimentally investigate the ABS spectrum of planar InAs/Al Josephson junctions as a function of superconducting phase difference, ϕ, across the junction, and magnetic field, $B_\parallel$, applied in the plane of the sample, parallel to the superconductor-normal interfaces. At $B_\parallel = 0$, the ABS spectrum is symmetric under phase inversion. A small magnetic field, $B_\parallel \simeq 60$ mT, results in an ABS spectrum with a pronounced phase asymmetry that becomes maximal at $B_\parallel \simeq 0.15$ T. At higher magnetic fields ($B_\parallel > 0.22$ T), we observe a sign reversal of the phase asymmetry corresponding to a negative diode effect. The regions of negative diode effect are correlated with a closure and reopening of the spectral gap, and the formation of zero-bias conductance peaks (ZBCPs) in the tunneling spectra for certain gate voltage settings.

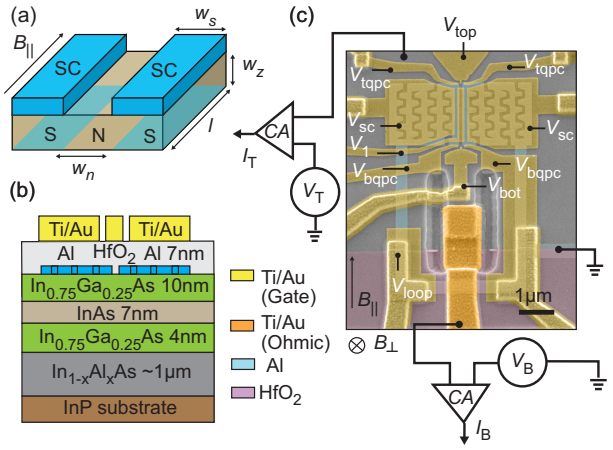

FIG. 1. Device schematic and micrograph. (a) Schematic of a planar Josephson junction device consisting of two superconducting leads (blue) of width $w_s = 1.8$ μm in epitaxial contact with the underlying semiconductor (brown). The normal region between the two leads is of width $w_n = 100$ nm, length $l = 1.6$ μm. The 2D electron wave function extends over a nominal thickness of $w_z \sim 20$ nm that includes the width of the InAs quantum well and the two insulating $In_{0.75}Ga_{0.25}As$ barriers. (b) Cross section of the device depicted schematically showing various layers comprising the heterostructure stack. Al (7 nm) is epitaxially grown on an $In_{0.75}Ga_{0.25}As$ (10 nm)/InAs (7 nm)/$In_{0.75}Ga_{0.25}As$ (4 nm) quantum well. Meandering perforations in the Al leads help with hardening of the superconducting gap. (c) False-colored electron micrograph of a planar Josephson junction device measured in a three-terminal configuration. dc biases, V_T and V_B, are applied to the top and bottom ohmics through current amplifiers connected to the respective terminals. The superconducting loop is grounded. An out-of-plane magnetic field $B_\perp$ threads magnetic flux through the superconducting loop for phase biasing. In-plane magnetic field $B_\parallel$ is applied in the plane of the device parallel to the S-N interfaces.

Based on numerical simulations, we interpret the observed phase asymmetry of the spectrum at low magnetic fields as a result of orbital coupling induced superconducting diode effect, similar to a mechanism proposed in recent works [13,28]. Within our model, at higher magnetic fields, an interplay of orbital and Zeeman coupling causes a sign reversal of the diode effect and is correlated with a topological phase transition of the junction.

The planar superconductor-normal-superconductor devices [Fig. 1(a)] are fabricated on InAs/Al two-dimensional heterostructures shown in Fig. 1(b), where Al plays the role of the parent superconductor (SC), and InAs is the semiconducting layer that serves as both the proximitized superconductor (S) where Al is present, and the normal (N) region of the junction where Al has been removed. The active semiconductor region, consisting of an InAs quantum well confined by $In_{0.75}Ga_{0.25}As$ barriers, has a thickness of $w_z \sim 20$ nm.

Figure 1(c) shows an electron micrograph of one of the devices, along with a schematic electrical circuit. The device geometry, fabrication method, and measurement setup has been discussed in detail in previous works [38,39]. Briefly, the Josephson junction device has a superconducting loop that connects the two superconducting leads, allowing phase-biasing by the application of a small (0.1 mT scale) out-of-plane magnetic field, $B_\perp$. Spectroscopy is performed by quantum point contacts (QPC) at both ends of the junction, formed by split gates that are controlled by voltages V_{tqpc} and V_{bqpc} at the top and bottom ends. The carrier density in the normal barrier is controlled by gate voltage V_1. We discuss results from Device 1 here; results from Device 2 and Device 3 are provided in the Supplemental Material [40].

We first focus on Device 1, where we performed tunneling spectroscopy only using the top QPC. At zero in-plane magnetic field, we observe a periodic modulation of the superconducting gap with period $B_\perp \simeq 0.16$ mT corresponding to one flux quantum $\Phi_0 = h/2e$ through the superconducting loop of area ~13 μm^2. Within each flux lobe, the gap modulation appears symmetric around maxima and minima, as shown in Figs. 2(a) and 2(g). This symmetry is broken by the application of $B_\parallel$. Already at $B_\parallel \simeq 0.06$ T [Fig. S4], the flux lobes are lopsided, with a smaller gap measured at the left end of the flux lobe compared to the right. The lopsidedness increases with $B_\parallel$, producing an arrowlike structure pointing toward the left end of the flux lobe, while the overall superconducting gap is also reduced [Fig. 2(b)]. Reversing the direction of the in-plane magnetic field reverses the direction of the arrow, as shown in the datasets at $B_\parallel = -0.14$ T [Fig. 2(f)] and $B_\parallel = +0.14$ T [Fig. 2(h)]. We speculate that small phase asymmetries at $B_\parallel = 0$ are due to an offset from residual fields in the magnet.

The asymmetric phase behavior persists until the spectral gap closes at $B_\parallel = B_c = 0.22$ T [Fig. 2(c)], where an X-shaped crossing of Andreev states is observed. Upon increasing the magnetic field further, the spectral gap reopens but with opposite phase asymmetry compared to the low-field spectra ($B_\parallel < B_c$) [Fig. 2(e)]. At the same time, for this particular setting of gate voltages, we observe the formation of a ZBCP that is stable with respect to phase variation [Figs. 2(d) and 2(e)].

An estimate of the supercurrent diode efficiency can be extracted from the phase-dependent Andreev spectra. The supercurrent carried by the junction is $I(\phi) = -2e/h \sum_i \delta E_i/\delta\phi \simeq -2e/h \int_{V_{SD}<0} (d\rho/d\phi)\epsilon d\epsilon$, with $E_i < 0$ the energy of an occupied Andreev level. We approximate the sum over energy levels as an integral over density of states $\rho(\phi)$, which can be obtained from the phase-dependent differential conductance [Fig. 2] up to an approximately constant factor relating differential conductance to density of states, as discussed in Ref. [51]. The ratio I^*_{c+}/I^*_{c-} of maximum (I^*_{c+}) and minimum (I^*_{c-}) estimated critical currents is then obtained from the current-phase

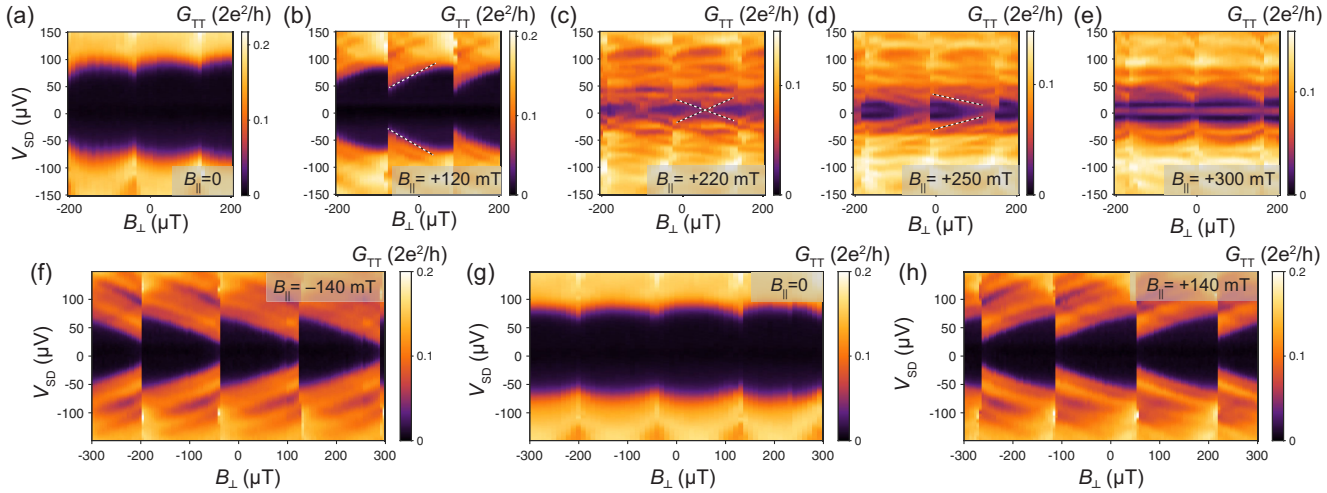

FIG. 2. Andreev bound state spectrum. (a) Differential conductance measured in Device 1 as a function of $B_\perp$ at different value of $B_\parallel$. At $B_\parallel = 0$, the Andreev bound state spectrum is phase-symmetric within each flux lobe. (b) For nonzero $B_\parallel$, the spectrum acquires an asymmetry within each flux lobe. (c) At a critical magnetic field $B_c = B_\parallel = 0.22$ T, the asymmetry disappears. (d),(e) At higher magnetic field ($B_\parallel > B_c$), the asymmetry reappears with an opposite sense and eventually disappears for an even higher field. (f)–(h) The sense of asymmetry within each flux lobe is opposite for $B_\parallel = +0.14$ T and (h) $B_\parallel = -0.14$ T. There is no asymmetry at (g) $B_\parallel = 0$. Top gate voltage $V_1 = 86$ mV.

relation (see Fig. S5), allowing us to estimate an approximate diode efficiency $\eta^* = (|I^*_{c+}/I^*_{c-}| - 1)/(|I^*_{c+}/I^*_{c-}| + 1)$. We plot η^* as a function of $B_\parallel$ in Fig. 3(a). We note that η^* agrees qualitatively, but may differ quantitatively from the diode efficiency $\eta = (|I_{c+}/I_{c-}| - 1)/(|I_{c+}/I_{c-}| + 1)$ of critical currents $I_{c\pm}$ in a current-biased measurement [25–29] (see Supplemental Material, Sec. I [40] for details).

The extracted diode efficiency η^* is near zero for $B_\parallel < +50$ mT, and rises sharply to a maximum of 0.6 at $B_\parallel \simeq +150$ mT, roughly tracking the phase asymmetry seen in Figs. 2(b) and S4. Further increase of $B_\parallel$ diminishes η^* until it reaches zero at $B_\parallel = B_c \simeq 220$ mT, where the spectral gap closes [Fig. 2(c)]. Thereafter, η^* changes sign, tracking the reversed phase asymmetry in Fig. 2(e). In this range, the gap reopens and a ZBCP is observed.

The correlation of the sign reversal of the phase asymmetry with the reopening of the spectral gap can be seen clearly by comparing the evolution of η^* with $B_\parallel$ in Fig. 3(a) with the variation of the spectrum in Fig. 3(b). At higher fields, $B_\parallel > 0.4$ T, the closing of the spectral gap is accompanied by a positive η^* before η^* is again suppressed as the gap fully closes. This variation of η^* is found for different gate voltage settings in Device 1 (see Fig. S6 [40]) including settings where the gap reopening is present but no ZBCP is observed [Figs. 3(c) and 3(d)]. Device 2 shows similar correlation between asymmetry, as measured by η^*, and the closing and reopening of the gap in the Andreev spectra (see Fig. S10 [40]). Additionally, three-terminal conductance spectroscopy in Devices 2 and 3 show that the phase-asymmetric ABSs extend throughout the bulk of the junction, as opposed to localized features associated only with the device ends [52–54] (see Supplemental Material, Sec. L [40] for details).

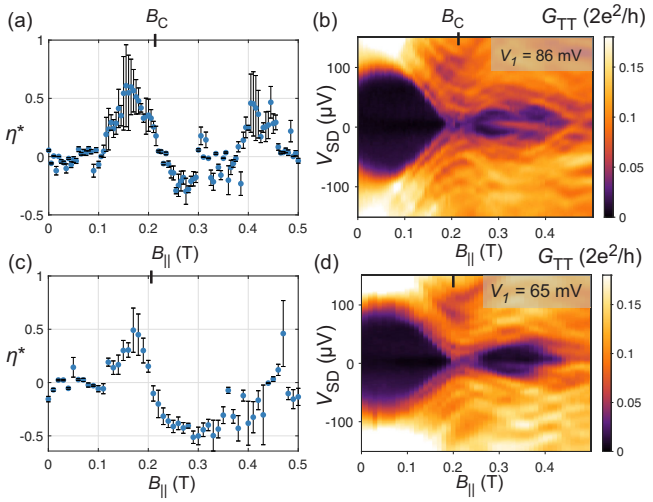

FIG. 3. In-plane field dependence. (a) Diode efficiency η^* estimated from the phase-dependent tunneling spectra. (b) Differential conductance measured as a function of $B_\parallel$ at the center of the flux lobe, corresponding to $\phi = 0$ at $B_\parallel = 0$. $B_c \simeq 220$ mT is the critical field at which the spectral gap closes. At the same field, we observe that η^* changes sign. Top gate voltage $V_1 = 86$ mV same as in Fig. 2. (c) η^* and (d) differential conductance spectrum at a top gate voltage setting ($V_1 = 65$ mV) where the gap-reopening signature is present without ZBCPs. The field range where $\eta^* < 0$ appears to be correlated with the reopening of the spectral gap in both cases.

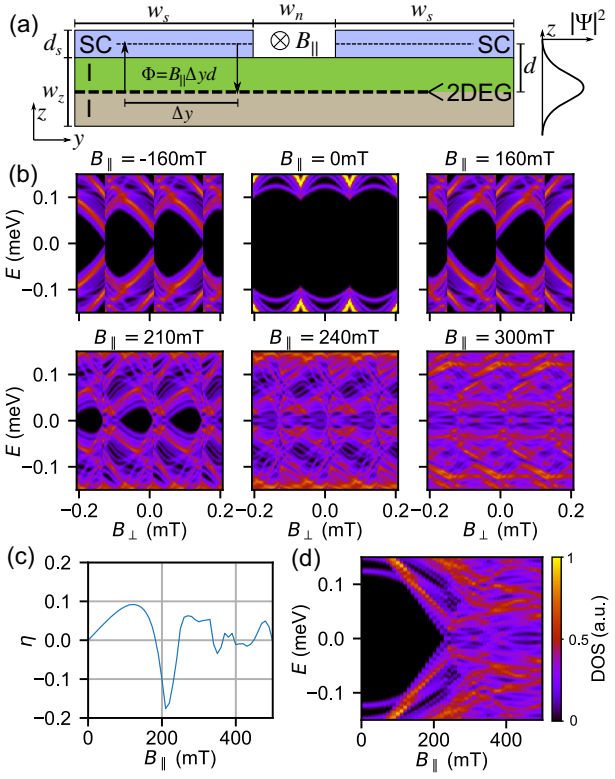

FIG. 4. Model and numerical results. (a) Sketch of the Josephson junction cross section formed by two superconducting films of width $w_s = 400$ nm and separation $w_n = 100$ nm deposited on top of a 2DEG with wave function profile $|\Psi|^2$ (sketch). The mean separation between the 2DEG and the superconductor is $d \sim 15$ nm. Cooper pairs in the proximitized 2DEG acquire a finite momentum $q = \pi B_\parallel d/\Phi_0$ from the flux $\Phi = B_\parallel d \Delta y$ enclosed by electron hopping between the layers at different positions Δy. (b) Calculated DOS with in-plane field $B_\parallel = -160$, 0, 160, 210, 240, and 300 mT (from top left to bottom right) with loop inductance $L = 1$ nH and a Gaussian linewidth of 30 μeV. (c) Critical current diode efficiency η. (d) DOS at equilibrium phase ϕ_0.

Finally, we note that the diode effect in Devices 1–3 showed weak top gate voltage (V_1) dependence (for example, see Fig. S6 [40]). On the other hand, we found a strong dependence of the diode effect on device geometry. In a device with narrow superconducting leads ($w_s = 160$ nm, Device S) studied in Ref. [55], the experimental diode efficiency η^* is maximal at $B_\parallel = 0.6$ T (see Fig. S7 [40]), compared to 0.15 T in devices with wide leads ($w_s = 1.8$ μm, Devices 1–3).

We turn to numerical simulation to better understand the experimentally observed nonreciprocity and its field dependence. The InAs quantum well is modeled as a two-dimensional electron gas (2DEG) with effective mass $m^* = 0.026 m_e$, chemical potential $\mu = 1.5$ meV [38,56], spin-orbit coupling $\alpha = 15$ meV nm, and g factor $g = -10$ in proximity to an Al superconducting layer with superconducting gap $|\Delta| = 0.2$ meV. In addition to spin-orbit and Zeeman interactions previously considered for diode physics [33,57–59], we now account for orbital effects, which are sizable for our device geometry. The thickness of the quantum well, $w_z = 20$ nm, and superconductor $d_s = 7$ nm, such that the 2DEG is located $d = (w_z + d_s)/2$–15 nm below the superconducting layer [Fig. 4(a)]. Electrons tunneling between the two layers acquire a geometric phase shift from the orbital coupling to the in-plane magnetic field $B_\parallel$. As a consequence, Cooper pairs in the proximitized 2DEG acquire a finite momentum perpendicular to the applied field. In the gauge $\vec{A} = -B_\parallel z \hat{e}_y$, the orbital coupling yields a phase gradient $\phi \to \phi + 2qy$ of the proximity-induced pairing $\Delta e^{i\phi}$ [60], where $q = \pi B_\parallel d/\Phi_0$ is the Cooper pair momentum arising from orbital effect alone [28] (see Supplemental Material, Sec. E for details [40]).

We first discuss the low-field behavior. Numerical density of states (DOS) as a function of phase bias at different $B_\parallel$ are shown in Fig. 4(b). At $B_\parallel = 0$, the DOS is symmetric. At $B_\parallel = \pm 0.16$ T, the spectrum is strongly nonreciprocal, with opposite asymmetries at opposite $B_\parallel$, consistent with Onsager microreversibility. The numerical DOS agrees well with the experimental phase spectra measured at low fields [Figs. 2(b), 2(f), and 2(h)]. The nonreciprocal spectrum can be further characterized by the calculated critical current diode efficiency η. As shown in Fig. 4(c), $\eta \simeq +8\%$ at $B_\parallel \simeq 160$ mT, roughly where the ABS spectrum is most phase-asymmetric, and also where η^* is maximal in the experiment [Fig. 3(a)].

For the material parameters used in the numerics, finite-momentum Cooper pairing dominates nonreciprocity (see Fig. S3 [40]), compared to effects of spin-orbit plus Zeeman couplings, which is the more commonly explored mechanism for nonreciprocity [33,57–59]. We note that nonreciprocal ABSs can be obtained in the numerics at low magnetic fields without including finite-momentum Cooper pairing, but this requires unreasonable values of g factor ($|g| \sim 60$) and spin-orbit coupling ($\alpha \sim 90$ meV nm), as discussed in the Supplemental Material, Sec. J [40]. Further, the weak gate-voltage dependence of η^* favors an orbital over a spin-orbit plus Zeeman mechanism, since the effect of spin-orbit coupling is expected to vary strongly with gate voltage (see Fig. S6 [40]). At the same time, the superconducting lead width (w_s) dependence of the magnetic field where η^* is maximized (150 mT for $w_s = 1.8$ μm and 600 mT for $w_s = 160$ nm) is consistent with an orbital effect mechanism that scales as the device cross section area $\propto (2w_s + w_n)w_z$ (see Fig. S7 [40]).

Now we discuss the high-field behavior of the numerics, where the contributions from spin-orbit plus Zeeman coupling become significant. The gap in the local density of states begins to close at $B_\parallel = 0.2$ T [Fig. 4(b)]. Further increase of field causes the gap to reopen ($B_\parallel = 0.25$ T) while a DOS peak appears at zero energy. This indicates a

topological phase transition of the junction where the zero-energy peak arises from a Majorana mode. This occurs simultaneously with a sign reversal of η [Figs. 4(c) and 4(d)]. The topological phase transition at the equilibrium phase bias ϕ_0 is caused by a fermion-parity transition of the $k_x = 0$ mode whereby the corresponding Andreev bound state crosses zero energy at $\phi = \phi_0$ as $B_\parallel$ is increased. After the crossing, the supercurrent carried by the Andreev bound state has a negative contribution that leads to the sign reversal of the diode effect (see Supplemental Material, Sec. H for details [40]). This behavior is consistent with experiment where we observed sign reversal of η^* associated with a reopening of the spectral gap and appearance of ZBCPs.

Qualitative agreement between experiment and numerics supports our interpretation of finite-momentum Cooper pairing arising from orbital coupling of the in-plane magnetic field as the dominant mechanism for the observed low-magnetic-field nonreciprocity. This mechanism does not rely on spin-orbit or Zeeman couplings, and suggests that other proximity-effect-based superconducting platforms such as graphene [61], Ge/SiGe [62], or GaAs [63] heterostructures, where these couplings are small or nonexistent, may host nonreciprocal superconductivity. At high magnetic field, we observe a sign reversal of the diode effect that has a possible topological interpretation. We note that two recent works on Josephson junctions on the same material platform (InAs/Al) reported a similar sign reversal of the diode effect [16,64]. The connection between finite-momentum Cooper pairing, nonreciprocal superconductivity, and topological superconductivity warrants further study [65,66].

Our calculations suggest that the sign-reversed diode effect can surpass the positive diode effect and even breach the previous theoretical limit of $|\eta| \approx 40\%$ [28]. Compatibility of our material platform with superconducting quantum computation architectures opens the possibility to integrate nonreciprocal Josephson junctions as three-wave mixing elements with essential applications as traveling-wave parametric amplifiers [67] and coherent-state generation for bosonic-encoded qubits [68]. Future work will focus on these directions.

We thank Constantin Schrade, Rubén Seoane Souto, Andreas Costa, Jaroslav Fabian, Denis Kochan, Nicola Paradiso, Simon Reinhardt, and Christoph Strunk for discussions, Geoff Gardner and Sergei Gronin for contributions to materials growth, Asbjørn Drachmann for assistance with fabrication, Antonio Fornieri and Alexander M. Whiticar for assistance with measurements. We acknowledge a research grant (Project 43951) from VILLUM FONDEN. M. G. acknowledges support by the European Research Council (ERC) under the European Union's Horizon 2020 research and innovation program under grant agreement No. 856526, and from the Deutsche Forschungsgemeinschaft (DFG) project grant 277101999 within the CRC network TR 183 (subproject C01), and from the Danish National Research Foundation, the Danish Council for Independent Research | Natural Sciences.

[1] J. Hu, C. Wu, and X. Dai, Phys. Rev. Lett. **99**, 067004 (2007).
[2] R. Wakatsuki, Y. Saito, S. Hoshino, Y. M. Itahashi, T. Ideue, M. Ezawa, Y. Iwasa, and N. Nagaosa, Sci. Adv. **3**, e1602390 (2017).
[3] F. Qin, W. Shi, T. Ideue, M. Yoshida, A. Zak, R. Tenne, T. Kikitsu, D. Inoue, D. Hashizume, and Y. Iwasa, Nat. Commun. **8**, 1 (2017).
[4] K. Yasuda, H. Yasuda, T. Liang, R. Yoshimi, A. Tsukazaki, K. S. Takahashi, N. Nagaosa, M. Kawasaki, and Y. Tokura, Nat. Commun. **10**, 1 (2019).
[5] Y. M. Itahashi, T. Ideue, Y. Saito, S. Shimizu, T. Ouchi, T. Nojima, and Y. Iwasa, Sci. Adv. **6**, eaay9120 (2020).
[6] F. Ando, Y. Miyasaka, T. Li, J. Ishizuka, T. Arakawa, Y. Shiota, T. Moriyama, Y. Yanase, and T. Ono, Nature (London) **584**, 373 (2020).
[7] L. Bauriedl, C. Bäuml, L. Fuchs, C. Baumgartner, N. Paulik, J. M. Bauer, K.-Q. Lin, J. M. Lupton, T. Taniguchi, K. Watanabe, C. Strunk, and N. Paradiso, Nat. Commun. **13**, 1 (2022).
[8] J. Yun, S. Son, J. Shin, G. Park, K. Zhang, Y. J. Shin, J.-G. Park, and D. Kim, Phys. Rev. Res. **5**, L022064 (2023).
[9] J. Diez-Merida, A. Díez-Carlón, S. Yang, Y.-M. Xie, X.-J. Gao, K. Watanabe, T. Taniguchi, X. Lu, K. T. Law, and D. K. Efetov, arXiv:2110.01067.
[10] J. Lin, P. Siriviboon, H. Scammell, S. Liu, D. Rhodes, K. Watanabe, T. Taniguchi, J. Hone, M. Scheurer, and J. Li, arXiv:2112.07841.
[11] A. Sundaresh, J. I. Väyrynen, Y. Lyanda-Geller, and L. P. Rokhinson, Nat. Commun. **14**, 1 (2023).
[12] A. A. Reynoso, G. Usaj, C. A. Balseiro, D. Feinberg, and M. Avignon, Phys. Rev. Lett. **101**, 107001 (2008).
[13] B. Pal, A. Chakraborty, P. Sivakumar, M. Davydova, A. Gopi, A. Pandeya, J. Krieger, Y. Zhang, S. Ju, N. Yuan *et al.*, Nat. Phys. **18**, 1228 (2022).
[14] H. Wu, Y. Wang, Y. Xu, P. K. Sivakumar, C. Pasco, U. Filippozzi, S. S. Parkin, Y.-J. Zeng, T. McQueen, and M. N. Ali, Nature (London) **604**, 653 (2022).
[15] C. Baumgartner, L. Fuchs, A. Costa, S. Reinhardt, S. Gronin, G. C. Gardner, T. Lindemann, M. J. Manfra, P. E. Faria Junior, D. Kochan *et al.*, Nat. Nanotechnol. **17**, 39 (2022).
[16] A. Costa, C. Baumgartner, S. Reinhardt, J. Berger, S. Gronin, G. Gardner, T. Lindemann, M. Manfra, J. Fabian, D. Kochan *et al.*, Nat. Nanotechnol. 1 (2023), 10.1038/s41565-023-01451-x.
[17] M. Gupta, G. V. Graziano, M. Pendharkar, J. T. Dong, C. P. Dempsey, C. Palmstrøm, and V. S. Pribiag, Nat. Commun. **14**, 3078 (2023).
[18] A. Zazunov, R. Egger, T. Jonckheere, and T. Martin, Phys. Rev. Lett. **103**, 147004 (2009).
[19] A. Brunetti, A. Zazunov, A. Kundu, and R. Egger, Phys. Rev. B **88**, 144515 (2013).

[20] T. Yokoyama, M. Eto, and Y. V. Nazarov, Phys. Rev. B **89**, 195407 (2014).
[21] C.-Z. Chen, J. J. He, M. N. Ali, G.-H. Lee, K. C. Fong, and K. T. Law, Phys. Rev. B **98**, 075430 (2018).
[22] R. Wakatsuki and N. Nagaosa, Phys. Rev. Lett. **121**, 026601 (2018).
[23] S. Hoshino, R. Wakatsuki, K. Hamamoto, and N. Nagaosa, Phys. Rev. B **98**, 054510 (2018).
[24] S. Pal and C. Benjamin, Europhys. Lett. **126**, 57002 (2019).
[25] J. J. He, Y. Tanaka, and N. Nagaosa, New J. Phys. **24**, 053014 (2022).
[26] S. Ilić and F. S. Bergeret, Phys. Rev. Lett. **128**, 177001 (2022).
[27] N. F. Yuan and L. Fu, Proc. Natl. Acad. Sci. U.S.A. **119**, e2119548119 (2022).
[28] M. Davydova, S. Prembabu, and L. Fu, Sci. Adv. **8**, eabo0309 (2022).
[29] A. Daido, Y. Ikeda, and Y. Yanase, Phys. Rev. Lett. **128**, 037001 (2022).
[30] R. S. Souto, M. Leijnse, and C. Schrade, Phys. Rev. Lett. **129**, 267702 (2022).
[31] B. Zinkl, K. Hamamoto, and M. Sigrist, Phys. Rev. Res. **4**, 033167 (2022).
[32] S. Ilić, P. Virtanen, T. T. Heikkilä, and F. S. Bergeret, Phys. Rev. Appl. **17**, 034049 (2022).
[33] A. Buzdin, Phys. Rev. Lett. **101**, 107005 (2008).
[34] K. N. Nesterov, M. Houzet, and J. S. Meyer, Phys. Rev. B **93**, 174502 (2016).
[35] D. Szombati, S. Nadj-Perge, D. Car, S. Plissard, E. Bakkers, and L. Kouwenhoven, Nat. Phys. **12**, 568 (2016).
[36] D. J. Van Woerkom, A. Proutski, B. Van Heck, D. Bouman, J. I. Väyrynen, L. I. Glazman, P. Krogstrup, J. Nygård, L. P. Kouwenhoven, and A. Geresdi, Nat. Phys. **13**, 876 (2017).
[37] L. Tosi, C. Metzger, M. F. Goffman, C. Urbina, H. Pothier, S. Park, A. L. Yeyati, J. Nygård, and P. Krogstrup, Phys. Rev. X **9**, 011010 (2019).
[38] A. Banerjee, O. Lesser, M. A. Rahman, H.-R. Wang, M.-R. Li, A. Kringhøj, A. M. Whiticar, A. C. C. Drachmann, C. Thomas, T. Wang, M. J. Manfra, E. Berg, Y. Oreg, A. Stern, and C. M. Marcus, Phys. Rev. B **107**, 245304 (2023).
[39] A. Banerjee, O. Lesser, M. A. Rahman, C. Thomas, T. Wang, M. J. Manfra, E. Berg, Y. Oreg, A. Stern, and C. M. Marcus, Phys. Rev. Lett. **130**, 096202 (2023).
[40] See Supplemental Material at http://link.aps.org/supplemental/10.1103/PhysRevLett.131.196301, which includes Refs. [41–50], for details of device fabrication, measurement, additional experimental data and theoretical modelling.
[41] J. R. Clem, Phys. Rev. B **81**, 144515 (2010).
[42] M. Tinkham, *Introduction to Superconductivity*, 2nd ed., International Series in Pure and Applied Physics (McGraw-Hill, New York, 1996).
[43] W. L. McMillan, Phys. Rev. **175**, 537 (1968).
[44] R. Meservey and P. M. Tedrow, J. Appl. Phys. **40**, 2028 (1969).
[45] C. W. Groth, M. Wimmer, A. R. Akhmerov, and X. Waintal, New J. Phys. **16**, 063065 (2014).
[46] M. Hell, M. Leijnse, and K. Flensberg, Phys. Rev. Lett. **118**, 107701 (2017).
[47] C. W. J. Beenakker, in *Transport Phenomena in Mesoscopic Systems* (Springer, Berlin, Germany, 1992), pp. 235–253.
[48] A. Haim and A. Stern, Phys. Rev. Lett. **122**, 126801 (2019).
[49] T. Laeven, B. Nijholt, M. Wimmer, and A. R. Akhmerov, Phys. Rev. Lett. **125**, 086802 (2020).
[50] J. A. van Dam, Y. V. Nazarov, E. P. A. M. Bakkers, S. De Franceschi, and L. P. Kouwenhoven, Nature (London) **442**, 667 (2006).
[51] F. Nichele, E. Portolés, A. Fornieri, A. M. Whiticar, A. C. C. Drachmann, S. Gronin, T. Wang, G. C. Gardner, C. Thomas, A. T. Hatke, M. J. Manfra, and C. M. Marcus, Phys. Rev. Lett. **124**, 226801 (2020).
[52] T. O. Rosdahl, A. Vuik, M. Kjaergaard, and A. R. Akhmerov, Phys. Rev. B **97**, 045421 (2018).
[53] J. Danon, A. B. Hellenes, E. B. Hansen, L. Casparis, A. P. Higginbotham, and K. Flensberg, Phys. Rev. Lett. **124**, 036801 (2020).
[54] A. Maiani, M. Geier, and K. Flensberg, Phys. Rev. B **106**, 104516 (2022).
[55] A. Fornieri, A. M. Whiticar, F. Setiawan, E. Portolés, A. C. Drachmann, A. Keselman, S. Gronin, C. Thomas, T. Wang, R. Kallaher *et al.*, Nature (London) **569**, 89 (2019).
[56] A. Banerjee, M. Geier, M. A. Rahman, D. S. Sanchez, C. Thomas, T. Wang, M. J. Manfra, K. Flensberg, and C. M. Marcus, Phys. Rev. Lett. **130**, 116203 (2023).
[57] T. Yokoyama, M. Eto, and Y. V. Nazarov, Phys. Rev. B **89**, 195407 (2014).
[58] F. Dolcini, M. Houzet, and J. S. Meyer, Phys. Rev. B **92**, 035428 (2015).
[59] C. Baumgartner, L. Fuchs, A. Costa, S. Reinhardt, S. Gronin, G. C. Gardner, T. Lindemann, M. J. Manfra, P. E. Faria Junior, D. Kochan, J. Fabian, N. Paradiso, and C. Strunk, Nat. Nanotechnol. **17**, 39 (2022).
[60] F. Pientka, A. Keselman, E. Berg, A. Yacoby, A. Stern, and B. I. Halperin, Phys. Rev. X **7**, 021032 (2017).
[61] G.-H. Lee, S. Kim, S.-H. Jhi, and H.-J. Lee, Nat. Commun. **6**, 1 (2015).
[62] G. Scappucci, C. Kloeffel, F. A. Zwanenburg, D. Loss, M. Myronov, J.-J. Zhang, S. De Franceschi, G. Katsaros, and M. Veldhorst, Nat. Rev. Mater. **6**, 926 (2021).
[63] Z. Wan, A. Kazakov, M. J. Manfra, L. N. Pfeiffer, K. W. West, and L. P. Rokhinson, Nat. Commun. **6**, 1 (2015).
[64] N. Lotfizadeh, B. Pekerten, P. Yu, W. Strickland, A. Matos-Abiague, and J. Shabani, arXiv:2303.01902.
[65] C. Qu, Z. Zheng, M. Gong, Y. Xu, L. Mao, X. Zou, G. Guo, and C. Zhang, Nat. Commun. **4**, 1 (2013).
[66] A. Melo, S. Rubbert, and A. Akhmerov, SciPost Phys. **7**, 039 (2019).
[67] N. E. Frattini, V. V. Sivak, A. Lingenfelter, S. Shankar, and M. H. Devoret, Phys. Rev. Appl. **10**, 054020 (2018).
[68] A. Grimm, N. E. Frattini, S. Puri, S. O. Mundhada, S. Touzard, M. Mirrahimi, S. M. Girvin, S. Shankar, and M. H. Devoret, Nature (London) **584**, 205 (2020).